International Journal of Modern Physics E
Vol. 29, No. 1 (2020) 2050002 (13 pages)

DOI: 10.1142/S0218301320500020

World Scientific
www.worldscientific.com

Pseudorapidity distributions of fast target protons in ^{32}S-Em collisions at Dubna energy

S. Kamel*,§, E. El-Falaky† and A. Saber‡

*Physics Department, Faculty of Education,
Ain Shams University, Cairo, Egypt

†Physics Department, Faculty of Science,
Suez University, El–Suez, Egypt

‡Mathematics and Physics Engineering Department,
Faculty of Engineering in Shoubra,
Banha University, Cairo, Egypt
§sayedks@windowslive.com

Received 3 October 2019
Revised 3 January 2020
Accepted 6 February 2020
Published 18 March 2020

In this paper, the possible mechanisms, which are responsible for the production of fast target fragments (gray particles with energy 26 up to 400 MeV) that were emitted from the interactions of ^{32}S nucleus with emulsion nuclei at energy 3.7 A GeV, are studied by the pseudorapidity distribution. The angular distribution of the fast protons (g-particles) emitted in the interactions of ^{32}S-Em at 3.7 A GeV is nicely described by exp (0.96 cos θ), which was observed in proton-induced interactions up to incident energies of 800 GeV. The pseudorapidity distributions of the produced g-particles were investigated in order to study the characteristics of the emitted system of g-particles for different target sizes (CNO, Em and AgBr groups of events). In all cases, the pseudorapidity distributions were parametrized using Gaussian fits. The temperature of the system emitting g-particles (hot system) is predicated in the light of the proposed statistical model to be $T \approx 60$ MeV.

Keywords: ^{32}S-Em interactions; fast target fragments; angular distribution; pseudorapidity distribution.

PACS Number(s): 25.75.−q, 25.70.Mn, 25.70.Pq, 29.40.Rg

1. Introduction

The multiplicity and pseudorapidity distributions of final-state particles can often be used to test various theoretical models and ideas. The rapidity distribution and the pseudorapidity distribution of charged particles are very important quantities when studying the mechanism of particle production in high energy nucleon–nucleon and nucleus–nucleus collisions.

A deeper insight into particle production mechanisms can be obtained from particle momenta distributions. Particle momenta are usually decomposed in the component transverse to the beam axis (p_T) and the one along the beam axis (p_L). In this way, all the information about the velocity of the particle-emitting source is contained in the longitudinal momentum, while the transverse momentum is free from kinematic effects and is governed only by the internal characteristics of the system that emits the particles.[1]

To study the longitudinal expansion, it is convenient to use the rapidity $y = \frac{1}{2}\ln\frac{E+p_L}{E-p_L}$ and pseudorapidity $\eta = -\ln(\tan\theta/2)$ variables, the latter being the approximation of the rapidity for large momentum particles. Pseudorapidity is more easily accessed experimentally because it requires the measurement of only one kinematic quantity for each particle (i.e., the polar angle (θ) with respect to the beam).

In the target fragmentation region, black (b-) and gray (g-) particles[2,3] are produced. The b-particles evaporate target protons with kinetic energy <30 MeV. The g-particles of interest are mainly recoiling protons knocked out from the target nucleus in the energy range 30–400 MeV. These g-particles are considered as fast target protons[4] produced during or shortly after the passage of the leading particles. Therefore, they are expected to carry most of the information from the earlier stages of the collision so the study of the emission characteristics of g-particles is of special significance. Although the process responsible for the production of these particles is not entirely known, it is generally believed that these are the low-energy part of the internuclear cascade, which is also supposed to carry information about the dynamics of the reaction because the time scale of emission of these particles is the same ($\approx 10^{-22}$ s) as shower particles produced. The investigation of these fragments is very useful for energy deposition and momentum transfer. The observations that are relevant to the nuclear limiting fragmentation also come from the experiments on target fragments. Therefore, Abdelsalam[5] suggested that the g-particles might be emitted from a thermalized system, within a short time, just after the earliest stage of the interaction that is associated with particle creation. In reflection, the created particles leave the hot hadronic matter formed in the overlap region between the projectile and target, as the earliest stage. In the first stage of the target fragmentation, the residual target part moves towards thermalization, where the fast target protons are emitted isotropically in the rest frame of the nucleus. In the second stage, which is the final interaction, the slow target protons are evaporated. The spectrum of the g-particle is exponential,[5] where the system moves towards equilibrium.

In light of the intranuclear cascade model[6–9] for the hadron–nucleus interaction, the emission of a g-particle may occur from the first strike of the target nucleon along the path of incidence as a first-generation or from the secondary cascading collision with lower momentum as a second generation. Therefore, this system also moves towards thermalization as explained in Refs. 5 and 10. More channels of

incident nucleons may be expected to result in more cascading through nucleus–nucleus interactions.

Pseudorapidity distribution is one of the most interesting experimental variables to investigate the mechanism of multiparticle production in hadronic and nuclear collisions. It is convenient for us to study the process of producing fast target fragments (g-particles) in the interactions of 3.7 A GeV Sulfur ions with nuclear emulsion by the pseudorapidity distribution. Based on the angular characteristics of these target fragments, the statistical thermodynamic model[10] is used to examine the fragmentation system.

2. Experimental Technique

This work is performed using emulsion stacks for 3.7 A GeV ^{32}S ions at Dubna Synchrophastron. To obtain high scanning efficiency, the pellicles were scanned under 100× magnification by doubly scanning along the beam tracks, fast in the forward direction and slow in the backward one. The details about the irradiation and scanning are found in Refs. 11 and 12. Once an interaction is observed, the incoming track is carefully examined to ensure that it is indeed a beam track. In the photographic nuclear emulsion, the tracks of secondary charged particles produced in each interaction can be classified according to their ionization range and velocity as follows:

(1) Black (b-) particles are those having a range of $L < 3$ mm corresponding to a proton with kinetic energy $\leq$26 MeV. Most of these are produced due to the evaporation of the residual target nucleus. The multiplicity of these slow target protons is denoted by n_b.
(2) Gray (g-) particles have $L \geq 3$ mm. These tracks are mostly due to protons of kinetic energy in the range 26–400 MeV and tracks of deuterons, tritons and slow mesons. The multiplicity of these fast target protons is denoted by n_g. In each event, the black and gray tracks together are called heavily ionizing tracks. Their multiplicity is denoted by $N_h = n_b + n_g$.
(3) Shower (s-) particles are singly charged relativistic particles. They are mostly fast pions with a small mixture of kaons and released protons from the projectile that have not undergone an interaction. Their multiplicity is denoted by n_s.

An event-by-event analysis demands the separation of events into ensembles of collisions of different projectiles with hydrogen (H), light nuclei (CNO) and heavy nuclei (AgBr). Usually, events with $N_h \leq 1$ are classified as collisions with hydrogen. Events yielding two to seven heavy tracks are classified as CNO events. Events with $N_h \geq 8$ arise from collisions with heavy nuclei, almost definitely belong to AgBr collisions. The particles produced in each event are also divided into particles emitted in the forward hemisphere (F) of the reaction ($\theta < 90^\circ$) and particles emitted in the backward one (B) ($\theta \geq 90^\circ$).

3. Experimental Results and Discussions

3.1. *Angular characteristics of g-particles*

We measured the mean angle of the emitted g-particles in ^{32}S-Em interactions at 3.7 A GeV ($\langle\theta_g\rangle = 55.75 \pm 2.50$). This value is displayed in Fig. 1 with the corresponding values from p, ^{4}He, ^{6}Li, ^{7}Li, ^{12}C, ^{16}O, ^{22}Ne, ^{24}Mg and ^{28}Si projectiles[13–16] at nearly the same energy. The dotted line is used as a guideline representing the average of mean angles at $\langle\theta_g\rangle \approx 60°$. From Fig. 1, we can observe that the mean angle of the emitted g-particles is nearly independent of the projectile mass number.

The angular distribution of the g-particles emitted in the ^{32}S-Em interactions at 3.7 A GeV is shown in Fig. 2. For the sake of comparison, the corresponding angular distribution of g-particles emitted in the ^{24}Mg-Em interactions[15] of the

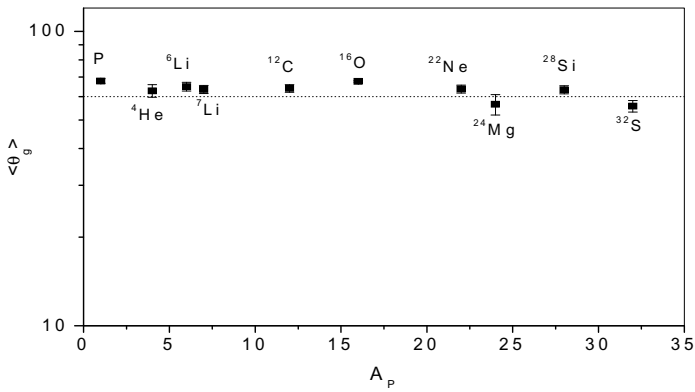

Fig. 1. Mean angle of the g-particles $\langle\theta_g\rangle$ emitted in the ^{32}S-Em interactions at 3.7 A GeV in comparison with the corresponding values for different projectiles at 2.1–3.7 A GeV. The dotted line represents a guideline at $\langle\theta_g\rangle \approx 60°$.

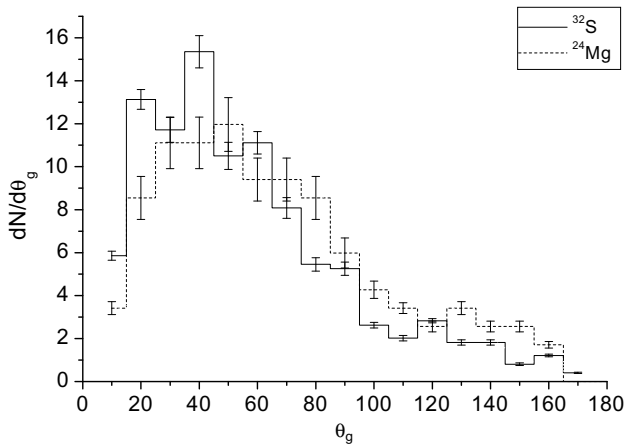

Fig. 2. Angular distributions of the g-particles emitted in the interactions of ^{32}S and ^{24}Mg with the emulsion nuclei at 3.7 A GeV.

same incident energy is displayed in the same figure as well. From this figure, one observes that the angular distributions of g-particles have a universal shape characterized by a forward peak. The numbers of the backward emitted particles (i.e., $\theta_g \geq 90°$) decrease with increasing θ_g. The distributions of such backward angles follow an exponential decay.

In Fig. 3, the angular distribution of the g-particles emitted in the ^{32}S-Em interactions at 3.7 A GeV can be fitted successfully using Gaussian distribution. Parameters and χ^2/DoF value of the Gaussian fit are shown in Table 1. In Fig. 3, our experimental data are also fitted by the predictions of Maxwell–Boltzmann statistics (MBS)[10] using the following relation:

$$\frac{dN}{d\theta}\alpha \sin\theta (F/B)^{\cos\theta}, \tag{1}$$

where F/B $(= 3.76 \pm 0.23)$ is the ratio of the number of g-particles in the forward hemisphere (F) to that in the backward one (B). This anisotropic factor leads one to investigate the target fragmentation system responsible for emitting g-particles in the framework of the statistical model that is based essentially on MBS. It is found that the MBS model predictions can reproduce the experimental data with slight underestimations (χ^2/DoF value equals 0.65).

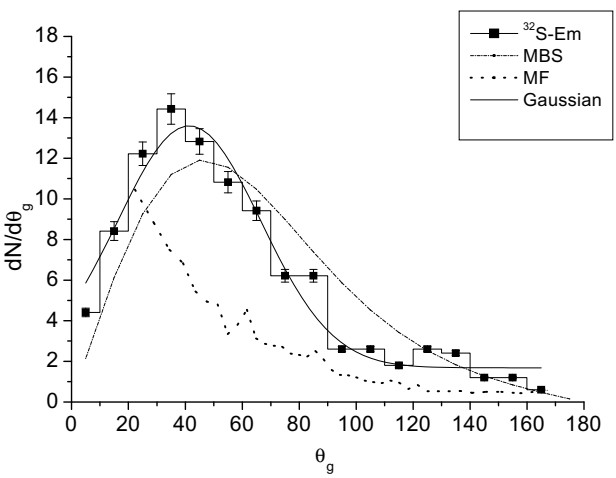

Fig. 3. Angular distribution of the g-particles emitted in the interactions of ^{32}S-Em at 3.7 A GeV fitted with Gaussian distribution and the predictions of MBS and MF models.

Table 1. Parameters and χ^2/DoF values of the Gaussian fit of angular distributions of g-particles measured for different target groups of events.

	$\langle\theta_g\rangle$	Width	Peak	Central value	χ^2/DoF
CNO	50.15 ± 5.04	44.65 ± 5.72	14.20	35.25 ± 2.35	0.25
Em	55.75 ± 2.50	50.26 ± 3.78	11.92	41.37 ± 1.48	0.07
AgBr	57.14 ± 2.86	53.11 ± 4.29	11.76	43.43 ± 1.68	0.08

We also compare our data in Fig. 3 with the corresponding data at 3.7 A GeV generated by the modified FRITIOF (MF) code.[17,18] The theoretical predictions of the MF model underestimate the data. Thus, it fails to describe the particle creation system for g-particles. The observed underestimation may be due to the probabilities of interactions with different components of the emulsion according to Glauber's approach.[19] Hence, the difference in model predictions is governed by different mechanisms of the multiparticle production process. However, a modern approach[20] in describing nuclear cascading may lead to better results.

To fulfill the investigation of the target size dependence, the present data are divided into two groups of events according to the accompanied N_h values. The angular distributions for g-particles emitted in the interactions of ^{32}S with (a) CNO and (b) AgBr at 3.7 A GeV are shown in Fig. 4. The experimental data are fitted successfully using the Gaussian model for both groups of events. The parameters

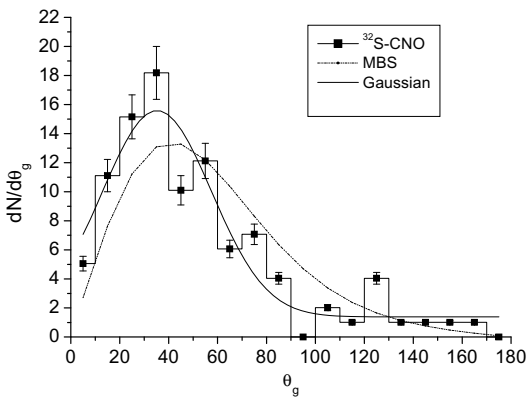

(a)

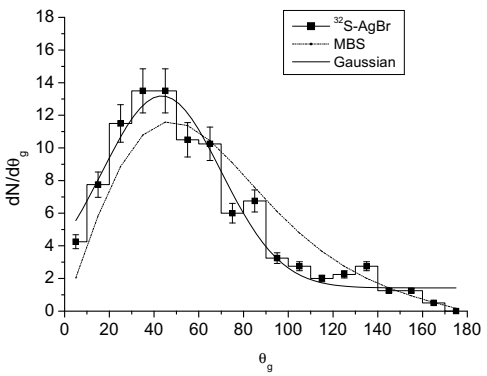

(b)

Fig. 4. Angular distributions for g-particles emitted with two different impact parameters (a) CNO and (b) AgBr in the 3.7 A GeV ^{32}S-Em interactions. Data are fitted with Gaussian distribution and MBS model predictions.

of the Gaussian fit are the width, the peak (the height of the curve's peak) and the central value (the position of the center of the peak) of the distribution. Parameters and χ^2/DoF values of the Gaussian fit for CNO and AgBr groups are shown in Table 1. The experimental data are also fitted by the prediction of the MBS model using the relation (1) for both groups (CNO and AgBr) with χ^2/DoF equal to 0.87 and 1.36, respectively.

In Ref. 21, it was found that the angular distribution in proton-induced interactions in the energy range 2–400 GeV has been parameterized as $e^{(0.96\cos\theta)}$. A fit to 800 GeV proton data[22] gives the same exponent. In Fig. 5, the angular distribution for the g-particles emitted in the interactions of ^{32}S at 3.7 A GeV with emulsion nuclei is plotted together with the line from Ref. 21 which represents the parameterization form above. Noticeably, our experimental results are reasonable as indicated by the line drawn where the χ^2/DoF value is 0.02. As a result, we can comment that the angular distributions of g-particles have an exponential universal shape. As noted in Ref. 23, the angular distribution of the g-particles in terms of emission angle appears independent of the variation of projectile mass, primary energy and target mass. In this regard, Adamovich[13] commented "*this is predicted in a simple picture where each participant nucleon in the target on the average gives the same contribution of g-particles independent of each other*".

In Fig. 6, the angular distribution for the gray tracks emitted in the interactions of ^{32}S-Em at 3.7 A GeV is compared with the corresponding experimental distributions with different N_h groups. The experimental data are well fitted by exponential function having the following form:

$$\frac{1}{N}\frac{dN}{d(\cos\theta_g)} \sim Ce^{(D\cos\theta_g)}. \tag{2}$$

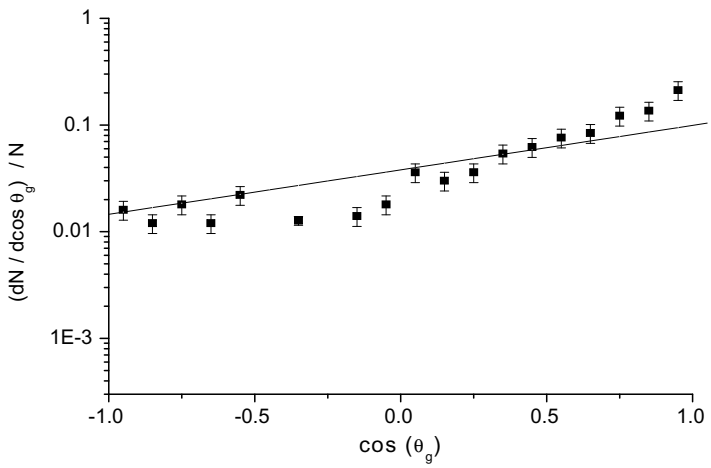

Fig. 5. Angular distribution of g-particles emitted in the interactions of ^{32}S-Em at 3.7 A GeV in comparison with the line from Ref. 21.

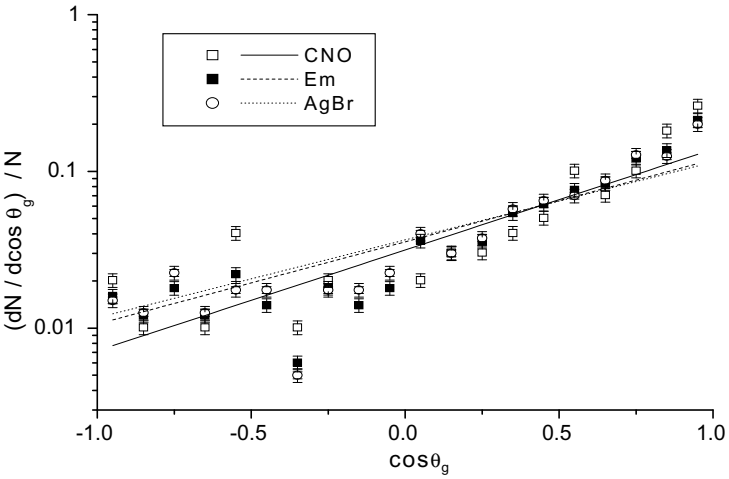

Fig. 6. Angular distributions of the g-particles emitted in the interactions of ^{32}S with CNO, Em and AgBr at 3.7 A GeV.

The value of D is determined by the amount of re-scattering in the target spectator.[24] In the absence of re-scattering, most recoil protons would go in the forward direction ($\cos\theta_g = 1$) and almost none in the backward direction ($\cos\theta_g = -1$). Thus, the slope D would be higher. Consequently, if there were significant re-scattering, the slope value would be lower. From the fitted curves, the values of D for Em, CNO and AgBr are calculated as 1.21 ± 0.25, 1.48 ± 0.24 and 1.14 ± 0.26 with values of χ^2/DoF 0.84, 1.39 and 0.75, respectively. One can notice that the D value for AgBr target is smaller than that for CNO and emulsion targets. Hence, in collision with heavy target (AgBr), g-particles suffer more re-scattering processes when compared to in collision with light ones (CNO). This may be due to the increase of cascading (secondary collisions) in the heavier target. It may be further concluded that gray tracks are emitted largely in the forward direction. The values of the F/B ratio of the angular distribution of g-particles are calculated and presented in Table 2. For comparison, the F/B ratios for different projectiles are also shown in the same table. A slight increase in the value of the F/B ratio with the projectile mass number is observed. This may be due to the increase in the number of primary collisions with increasing projectile size. On the other hand, the F/B ratio decreases with the target size (increasing cascading) which means that B increases relative to F.[25]

3.2. *Pseudorapidity distribution of g-particles*

Pseudorapidity distribution of the secondary particles emitted in high-energy nucleon–nucleus and nucleus–nucleus interactions contain significant information of the target and projectile fragmentation. The η values are quasi-invariant and easily defined ($\eta = -\ln\tan\theta/2$) in the emulsion experiment via the polar angle (θ).

Table 2. The ratio F/B of angular distributions of g-particles for different projectiles.

Projectile	Energy A GeV	F/B	Ref.
p-Em	3	3.36 ± 0.20	26
^{4}He-Em	3.7	3.00 ± 0.10	26
^{12}C-Em	3.7	4.69 ± 0.18	27
^{28}Si-Em	3.7	5.29 ± 0.24	27
^{32}S-CNO	3.7	8.00 ± 0.81	This work
^{32}S-Em		5.65 ± 0.25	
^{32}S-AgBr		5.25 ± 0.26	

Now, the pseudorapidity distribution of g-particles emitted in the interactions of 3.7 A GeV ^{32}S with nuclear emulsion is shown in Fig. 7. The distribution is fitted with a Gaussian function. The half-width value of the distribution obtained from the Gaussian fit is 0.69 ± 0.04. The pseudorapidity distribution has a peak at $\eta = 0.84$, 0.04.

To study the characteristics of the emitted system of g-particles concerning different target sizes, the present data are then divided into two groups of events according to the accompanied N_h values. Events with $2 \leq N_h \leq 7$ and $N_h \geq 8$ are taken to be due to interactions with CNO and AgBr groups, respectively. The events with $N_h \leq 1$ classified as interactions with hydrogen are not included in data analysis. Because the hydrogen nucleus has only one proton, its fragmentation results in an emission of one proton at most, as gray or black particles. Consequently, the multiplicity channels in the interactions with H are restricted to $N_h = 0$ or 1 only. The corresponding pseudorapidity distributions together with their Gaussian fitting are drawn in Fig. 7. The Gaussian peak is positioned at $\eta = 1.03 \pm 0.03$ for

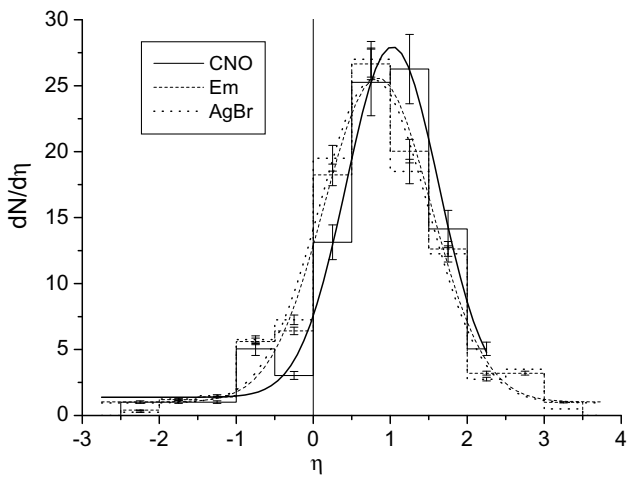

Fig. 7. Pseudorapidity distribution of g-particles emitted in ^{32}S interactions with CNO, Em and AgBr at 3.7 A GeV.

CNO group and 0.78 ± 0.04 for AgBr group. The half-width values are found to be 0.63 ± 0.02 and 0.70 ± 0.05, respectively.

From Fig. 7, the main features characterizing the pseudorapidity distributions are as follows:

(1) The peaking shape, where the peak occurs in the forward pseudorapidity region.
(2) The well-fitting by Gaussian distributions.
(3) The pseudorapidity ranges are from -2.5 to $+3.5$.

From the present data, one can notice the following:

(1) The half-width measured in all pseudorapidity distributions has approximately the same value. This may be due to the fixed energy range for the g-particles ($30 < E < 400\,\text{MeV}$), which results in the same angular spread for all groups of interactions.[27,28]
(2) The shift of peak position to the zero-point pseudorapidity distributions decreases with increasing N_h. This may be due to the increase of cascading collisions in the heavier target.
(3) The ratio F/B seems to decrease with increasing the target size. This could be because the larger the target size, the more cascading collisions leading to the increase of the emission of g-particles in the backward direction relative to the forward one (F/B ratio decreases).

In light of the statistical model,[10] based on the modification of MBS model,[29] the g-particles emitting system can be distinguished by main parameters, such as the mean longitudinal velocity of the center of mass of the particle emitting system ($\beta_{//}$), the characteristics spectral velocity of the fragmentation system of g-particles (β_o), and the temperature (T) associated with the emission system. In the rapidity curve, the value of $\beta_{//}$ is found from the peak position shift for the zero-point rapidity distribution. β_o can be obtained from the half-width (σ) of the rapidity distribution, where $\sigma^2 = \beta_o^2/2$. The temperature T in units of MeV can be found as $T = M_n\sigma^2$, where M_n is the nucleon rest mass.

In Ref. 5, Abdelsalam concludes that the standard deviations σ for all g-particles' rapidity distributions are the same within experimental errors with an average value $\sigma = 0.25 \pm 0.01$ (i.e., σ is independent of the target and projectile size). Besides, the rational value of the velocity $\chi = \beta_{//}/\beta_o$ appears to be constant, independent of projectile mass and energy of the fragments according to limiting fragmentation hypothesis.

It was also pointed out in Ref. 30 that the F/B ratio represents the rational value of the velocity $\chi^0 = \beta_{//}/\beta_o$ of the angular distribution[31] and was determined as

$$\chi^{01} = \beta_{//}/\beta_o \approx (\sqrt{\pi}/4)\ln(F/B). \tag{3}$$

The F/B ratio is also related to the angular distribution of the emitted g-particles fitted by the MBS model (Eq. (1)). The rational velocity values can

Table 3. Rational velocity and longitudinal velocity for different target groups of ^{32}S-Em interactions at 3.7 A GeV.

	F/B	$\langle\theta_g\rangle$	χ^{01}	χ^{02}	$\beta_{//1}$	$\beta_{//2}$
CNO	5.59 ± 0.69	50.15 ± 5.04	0.750	0.641	0.263	0.224
Em	3.76 ± 0.23	55.75 ± 2.50	0.586	0.563	0.205	0.197
AgBr	3.41 ± 0.19	57.14 ± 2.86	0.544	0.543	0.190	0.190

also be calculated from the experimental value of the mean emission angle $\langle\theta_g\rangle$ in Ref. 32

$$\chi^{02} = \beta_{//}/\beta_{\rm o} \approx \cos\langle\theta_g\rangle. \tag{4}$$

The rational velocity values for ^{32}S interactions with CNO, Em and AgBr calculated from Eqs. (3) and (4) are shown in Table 3. The χ^0 values can be compared with the experimental ones obtained from the rapidity curve[15] for ^{24}Mg. The χ^0 values for ^{24}Mg interactions with CNO, Em and AgBr are 0.715, 0.597 and 0.567, respectively. Knowing that βo ($\approx$0.35) is constant,[33] the values of longitudinal velocity $\beta_{//}$ for ^{32}S with CNO, Em and AgBr are calculated and displayed in Table 3. This table illustrates the values of F/B, $\langle\theta_g\rangle$, χ^0 and $\beta_{//}$ for our data. From this table, one can notice that:

(1) The χ^0 values deduced from Eq. (4) using the experimental values of the mean emission angle show a good agreement with the values deduced using the F/B ratios. The χ^0 values from the rapidity distributions of ^{24}Mg agree with our experimental data.
(2) The longitudinal velocity of the g-particle emitting system $\beta_{//}$ decreases with increasing the target size. This idea may be due to the increase of cascading collisions in the heaviest target.
(3) Based on the predictions of the modified statistical model, Abdelsalam *et al.*[5] found that the longitudinal velocity of the g-particle emission system was in the range of $\beta_{//} = 0.16$–0.23 using the rapidity distributions. This result corresponds to the current values of $\beta_{//}$ obtained experimentally by F/B ratios and $\langle\theta_g\rangle$ values.

Based on the above, the temperature of the emitting system can be calculated from the equation

$$T = M_n\sigma^2 \approx M_n(\beta_{\rm o}^2/2). \tag{5}$$

Knowing that $\beta_{\rm o} \approx 0.35$, the temperature of the g-particle emission system is $T \approx 60$ MeV. This value is consistent with those obtained before.[29,33]

4. Conclusion

In this work, the possible mechanisms which are responsible for the production of fast target fragments (g-particles with energy 26 up to 400 MeV) that emitted from

interactions of ^{32}S nucleus with emulsion nuclei at energy 3.7 A GeV are investigated. Based on the results of this study, let us summarize our main results as follows:

(1) The inspection of the mean angles of the emitted g-particles from different projectiles at Dubna energy reveals that the mean angle is nearly independent of the projectile mass number.
(2) The angular distribution for the fast protons emitted in the interactions of ^{32}S-Em at 3.7 A GeV is nicely described by exp $(0.96 \cos\theta)$, which was observed in proton-induced interactions up to incident energies of 800 GeV. This observation reveals that the angular distribution of g-particles is energy independent and seems to be independent of the projectile.
(3) The experimental angular distributions of g-particles at different N_h groups are well fitted by an exponential function and have the form $\frac{1}{N}\frac{dN}{d(\cos\theta_g)} \sim Ce^{(D\cos\theta_g)}$, where the value of D is determined by the amount of re-scattering in the target spectator.
(4) The D value for collisions with heavy targets is found to be smaller than its value for collisions with light targets. So, in collisions with heavy targets, g-particles suffer more scattering processes as compared to light ones. This may be due to the increase of cascading in the heavier target.
(5) The pseudorapidity distribution of the emitted g-particles is fitted with a Gaussian function, having a half-width equal to 0.69 ± 0.04 and peak at $\eta = 0.84 \pm 0.04$.
(6) The pseudorapidity distributions of the produced g-particles is investigated also to study the characteristics of the emitted system of g-particles for different target sizes (CNO and AgBr groups of events), revealing that the Gaussian peak is positioned, respectively, at η equal to 0.84 ± 0.04 and 0.78 ± 0.04. The half-width values are found to be 0.63 ± 0.02 and 0.70 ± 0.05, respectively.
(7) The χ^0 values deduced from the mean emission angle show good agreement with the values deduced from the F/B ratios. The χ^0 values from the rapidity distributions of g-particles induced by 3.7 A GeV of ^{24}Mg agree with our experimental data.
(8) The longitudinal velocity of the g-particle emitting system $\beta_{//}$, decreases with increasing the target size. This may be due to the increase of cascading collisions in the heaviest target.
(9) The temperature of the system emitting g-particles (hot system) is predicated in the light of the proposed statistical model to be $T \approx 60$ MeV.

Acknowledgments

The authors appreciate the guidance and advice given by Prof. Dr. A. Abdelsalam, head of Mohamed El–Nadi high energy Laboratory, Cairo University, where this work has been carried out. We owe much to Veksler and Baldin High Energy

Laboratory, JINR, Dubna, Russia, for supplying us with the photographic emulsion plates.

References

1. F. Prino, arXiv:0712.0357v1 [nucl-ex].
2. C. F. Powell, F. H. Fowler and D. H. Perkins, *The Study of Elementary Particles by the Photographic Method* (Pergamon Press, London, New York, Paris, Los Angles, 1958), p. 474.
3. H. Barkas, *Nuclear Research Emulsion*: *Technique and Theory*, Vol. 1 (Academic Press, Cambridge, 1963).
4. M. S. El–Nagdy, *Phys. Rev. C* **47** (1993) 346.
5. A. Abdelsalam, *Phys. Scr.* **47** (1993) 505.
6. V. I. Bubnov *et al.*, *Z. Phys. A*, *At. Nucl.* **302** (1981) 133.
7. M. K. Hegab and J. Hufner, *Phys. Lett. B* **105** (1981) 103.
8. M. K. Hegab and J. Hufner, *Nucl. Phys. A* **384** (1982) 353.
9. M. Tosson *et al.*, *Z. Phys. A*, *Hadrons Nuclei.* **347** (1994) 247.
10. H. H. Heckman *et al.*, *Phys. Rev. C* **17** (1978) 1651.
11. M. EI-Nadi *et al.*, *J. Phys. G*, *Nucl. Part. Phys.* **28** (2002) 241.
12. M. EI-Nadi *et al.*, *Int. J. Mod. Phys. E* **6** (1997) 191.
13. M. I. Adamovich *et al.*, *Phys. Lett. B* **230** (1989) 175; M. M. Sherif *et al.*, *Int. J. Mod. Phys. E* **2**, 835 (1993).
14. J. R. Florian *et al.*, Report Submitted to the Meeting of Division of Particles Fields, Berkeley, California, p. 1073.
15. A. Abdelsalam *et al.*, *Radiat. Phys. Chem.* **91** (2013) 1.
16. BWDKLMT Collab., *Sov. J. Nucl. Phys.* **29** (1979) 52.
17. B. Andersson *et al.*, *Nucl. Phys. B* **281** (1987) 289.
18. B. Nilsson-Almquist and E. Stenland, *Comput. Phys. Commun.* **43** (1987) 387.
19. S. Y. Shmakov and V. V. Uzhinskii, *Comput. Phys. Commun.* **54** (1989) 125.
20. V. Uzhinskii, in *Joint Int. Conf. on Supercomputing in Nuclear Application and Monte Carlo 2010* (*SNA + MC 2010*), Hitotsubashi Memorial Hall, Tokyo, Japan 17–21 October 2010, https://geant4.web.cern.ch/sites/geant4.web.cern.ch/files/geant4/results/papers/Firitof-MC2010.pdf.
21. I. Otterlund *et al.*, *Nucl. Phys. B* **142** (1978) 445.
22. A. Abduzhamilov *et al.*, *Phys. Rev. D* **39** (1989) 86.
23. A. El-Naghy, *IL Nouvo Cimento A* **71** (1982) 245 and references therein.
24. WA80 Collab. (R. Albrecht *et al.*), *Phys. Lett. B* **307** (1993) 269.
25. A. Dabrowska *et al.*, *Z. Phys. C* **59** (1993) 399.
26. M. A. Ahmed and S. Ahmed, *Ukr. J. Phys.* **57** (2012) 1205, ISSN 2071-0194 and reference therein.
27. O. Badawy *et al.*, *Z. Phys. A* **279** (1976) 408.
28. H. H. Heckman *et al.*, *Phys. Rev. Lett.* **28** (1972) 926.
29. M. El-Nadi *et al.*, *IL Nuovo Cimento* **107A** (1994) 31 and references therein.
30. M. EI-Nadi *et al.*, *Eur. Phys. J. A* **3** (1998) 183.
31. H. H. Heckman *et al.*, *Phys. Rev. C* **17** (1978) 1735.
32. M. EI-Nadi *et al.*, *Phys. Rev. Lett.* **52** (1984) 1971.
33. J. V. Geaga *et al.*, *Phys. Rev. Lett.* **45** (1980) 1993.